ELSEVIER

Coastal Engineering 30 (1997) 1–22

COASTAL ENGINEERING

# A laboratory study of longshore currents over barred and non-barred beaches

A.J.H.M. Reniers *, J.A. Battjes

*Delft University of Technology, Faculty of Civil Engineering, Delft, The Netherlands*

Received 25 September 1995; accepted 12 June 1996

## Abstract

A detailed description is given of the results of laboratory experiments on wave-driven longshore currents on both barred and non-barred beaches. The objective is to examine the cross-shore distribution of the longshore current velocities for purely wave-driven currents, with emphasis on the position of maximum current velocity with respect to areas where wave energy is dissipated. Unidirectional obliquely incident waves, both regular and random, were used. The measurements were performed in a large wave basin with a pump recirculation system to create spatially homogeneous longshore currents. The experiments yielded information on wave transformation, set-up of the mean water level and the cross-shore distribution of wave-driven longshore current velocity. A number of cases are presented and compared with each other. The measurements show that in the case of purely wave-driven longshore currents, the maximum current velocities occur close to areas where wave breaking is most intense. The effect of mixing, bottom friction and wave rollers on the longshore current velocity profile are examined in more detail with help of numerical modelling. Existing model equations, based on the assumption of alongshore uniformity, are used. The results for the mean longshore current profile on a barred beach are in close agreement with the measurements.

*Keywords:* Modelling; Longshore currents; Barred profile; Non-barred profile; Measurements

* Corresponding author. Fax: +31 15 2858582. E-mail: ad.reniers@wldelft.nl



*PII* S0378-3839(96)00033-6

## 1. Introduction

The longshore current is one of the main features in the surfzone. Its importance in coastal processes has long been established and much research has been done to model the longshore current velocity accurately. Comparison of model results with both field (Thornton and Guza, 1986; Church and Thornton, 1993, among others) and laboratory data (Visser, 1984; Svendsen and Putrevu, 1994, among others) for wave-driven longshore currents on planar beaches show in general good agreement. However, there has been much discussion on the cross-shore distribution of the wave-driven alongshore current velocity on barred beaches. In the case where field measurements show a maximum longshore current velocity in the trough, as observed during the DELILAH field experiment (Birkemeier, 1991) at Duck, North Carolina, numerical model studies for uniform longshore currents show that the maximum is near the bar crest with another maximum close to the shore line, corresponding to the locations where wave breaking occurs. Note that not all field measurements show this kind of longshore current velocity distribution (Whitford and Thornton, 1996).

Several mechanisms have been examined to explain this difference in behaviour, including turbulence effects (Church and Thornton, 1993), rollers (Lippmann et al., 1995), shear instabilities (Church and Thornton, 1993) and alongshore pressure gradients (Putrevu et al., 1995). In the authors' opinion, all the effects mentioned previously with the exception of the alongshore pressure gradient can at most cause a relatively minor shift of the velocity maximum away from the bar crest. They are not believed to contain a mechanism which would cause the maximum velocity to occur in the trough. Only the pressure gradient is such a mechanism. The fact that such gradient has not been observed in the field does not exclude it from being a likely cause, simply because a very weak gradient, too weak to be observable under normal conditions, suffices to generate a current with significant velocities.

The purpose of the present paper is to investigate the preceding matter experimentally. The measurement data presented here are part of a laboratory experiment on the generation and development of shear instabilities in uniform wave-driven longshore currents (Reniers et al., 1994). An important part of this experiment was to establish longshore currents in the wave basin which are uniform alongshore prior to monitoring shear instabilities. So in addition to the shear instability data, it yielded detailed information on the cross-shore distributions of wave-driven longshore currents in absence of an alongshore pressure gradient. These have been measured on both barred and non-barred beaches. In view of the discussion on the position of the maximum current velocity in relation to the areas where wave energy is being dissipated by breaking, we feel that the measurements on the cross-shore distribution of the longshore current velocity are valuable enough to be presented separately. The results can be used to obtain a better understanding of the forcing of wave-driven currents in the field.

This paper is organised as follows. First we discuss the experimental procedure to establish uniform longshore currents. Next the results obtained for the cross-shore distribution of the time-averaged longshore velocity for the various test conditions are presented and discussed. After that, model equations are introduced and a comparison is made of computed values with the measurements, thereby assessing the effects of bottom shear stress, rollers and lateral mixing. In the comparison of numerical results with measurements attention is focused on random waves because most often these conditions are a better approximation of what happens in the field.

## 2. Test set-up

The measurements were performed in a large wave basin, approximately 25 m wide by 40 m long. The test set-up is similar to the one used by Visser (1980). A pump system was used to recirculate the wave driven longshore current in order to obtain alongshore uniformity (in particular the absence of an alongshore pressure gradient). The layout is shown in Fig. 1. The beach has been rotated with respect to the wave maker to increase the length of the beach. Unidirectional obliquely incident waves, both regular and random, were generated by a multipaddle type wave maker. In the present tests, the wave paddles were kept in phase, together operating as a single wave maker.

Wave guides were used to prevent the waves from diffracting, thus avoiding alongshore variation of the wave set-up. The inflow opening was constructed in such a way that the pumped discharge could be distributed in correspondence with the measured longshore current velocity profile further downstream, thereby increasing the length over which the current was uniform. The width of the outflow opening could be changed by extending the wave guide.

The cross-shore distribution of the longshore current velocity was measured with eight electromagnetic flow meters (EMF) mounted on a mobile carriage. The instruments showed a good linear response up to 1.1 m/s with errors of the order of 1 cm/s. The current velocity measurements were located at one third of the water depth from the bottom, which is near the elevation of the depth-averaged current velocity in the case of a logarithmic velocity profile. During the experiment, the carriage could be moved along the beach, thus giving the possibility to measure in any transect between the inflow and

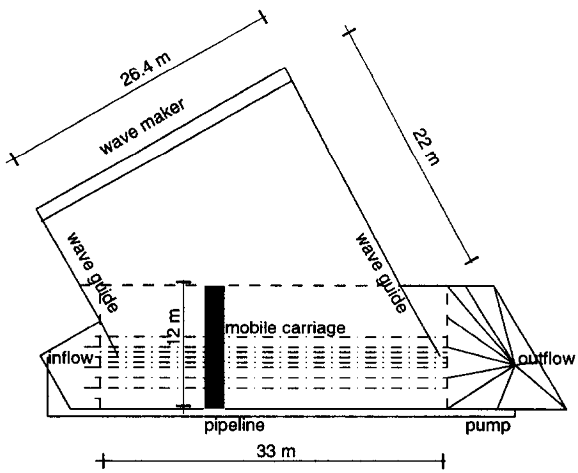


Fig. 1. Basin layout; the dash-dotted lines indicate the position of the bar.

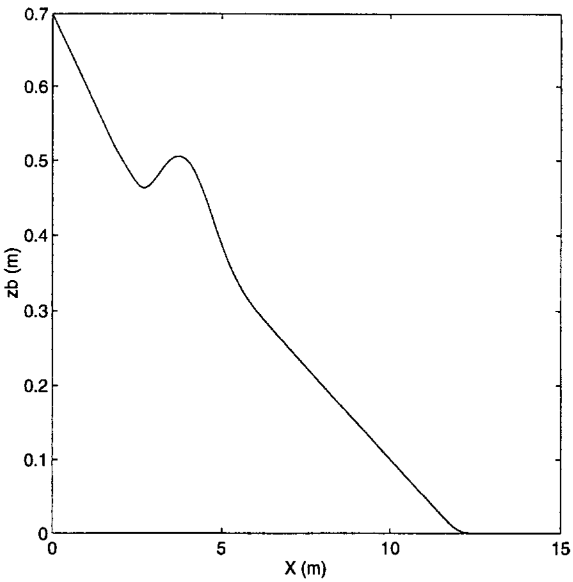


Fig. 2. Bottom profile.

outflow openings. Both dye and floaters were used to monitor the current velocity field in the basin and check uniformity.

Ten resistant type wave gauges were also mounted on the carriage to monitor the wave transformation and set-up of the mean water level, with a linear response up to 20 cm with an accuracy in the mean water level of O(1) mm.

The measurements were performed on a barred concrete slope with a 1 : 20 slope offshore (Fig. 2) on which a Gaussian bar profile with a crest height of about 0.1 m was superimposed, resulting in a slope of approximately 1 : 8 on the seaward side of the bar. The Gaussian bar profile was selected to reflect conditions observed in nature, with intense wave breaking over the bar, followed by waves reforming in the trough and additional wave breaking near the shoreline. Numerical modelling was used prior to the experiments to determine the desired crest height and bar width for the wave conditions under consideration. Shoreward of the bar, a plane 1 : 10 slope extended to an elevation above the expected run-up. Lowering the water level below the bar crest, to a level where overtopping of the bar did not occur, allowed measuring the current on a non-barred beach. The roughness of the smooth concrete bottom is estimated at $k_s = 0.0005$ m. For a more detailed description of the test set-up refer to Reniers et al. (1996).

## 3. Recirculation

The flow at a given transect is a combination of the pumped discharge and the recirculation in the basin. Visser (1980, 1991) showed that a minimum recirculation in the basin corresponds to an alongshore uniform wave driven current. His argument is as follows.

Table 1
Test conditions. $d$: mean water level, $H$: wave height, $T$: wave period

| Test description | test | $d$ (cm) | $H$ (cm) | $T$ (s) |
|---|---|---|---|---|
| regular waves + barred beach | SA243 | 55.0 | 8.0 | 1.0 |
| regular waves + barred beach | SA537 | 55.0 | 8.0 | 2.0 |
| random waves + barred beach | SO014 | 55.0 | 7.0 | 1.2 |
| regular waves + barred beach | SA337 | 55.0 | 10.0 | 1.0 |
| regular waves + non-barred beach | SC219 | 45.0 | 8.0 | 1.0 |

The recirculation is, in theory, zero when the pumped discharge is equal to the discharge forced by the waves. However, due to lateral mixing, a small recirculation remains. If the pumped discharge is too small, part of the wave driven flow is forced to recirculate in the basin. In case the pumped discharge is too large, this also results in a recirculation due to convection and lateral friction.

For each test condition (Table 1), the following had to be established to obtain a longshore uniform current:

- width of the outflow opening
- the optimal pumped discharge corresponding to a wave driven current only
- redistribution of the pumped discharge at the inflow opening

If the width of the outflow opening was too large, a double recirculation cell would occur in the case of a barred beach, irrespective of the fact whether the pumped discharge matched the wave-driven discharge or not. To avoid this, the wave guide would be extended just into the surfzone, forcing the excess flow in the main basin to deeper water near the outflow opening, resulting in a single recirculation cell. Further decreasing the width causes the flow to contract towards the downstream end of the basin, thereby decreasing the length over which the flow is uniform.

Once the width of the outflow opening was established, the uniformity of the longshore current was checked by a visual check of the recirculation in the basin, using dye or floaters, in combination with the measured cross-shore distribution of the longshore current velocity in four transects along the beach. Velocities were measured for 5 minutes in each transect (increasing the sample time beyond this value proved to give negligible differences in the measured mean, both for monochromatic and random waves).

In the case where the pumped discharge was not near the optimal discharge, a strong offshore directed flow would occur along the wave guide at the downstream end of the basin. This could easily be observed using the floaters and/or dye. The velocity measurements would show whether or not the distribution of the pumped discharge at the inflow opening had to be adapted. After each change in the basin configuration, the wave and current field were allowed to adapt for half an hour, after which the velocity field was measured again to check uniformity.

The preliminary data analysis was almost real time, so results could be checked immediately after the measurements had been performed, resulting in an efficient process to establish alongshore uniform currents.

## 4. Results

The test conditions are given in Table 1. The angle of wave incidence was 30° for all wave conditions. For brevity, not all the measurement data have been presented, but only typical results are presented and discussed.

### 4.1. Barred profile

The results for test SA243, regular obliquely incident waves of 8 cm height and 1 second wave period, are shown in Fig. 3. The results obtained from the first wave gauge offshore are not shown. Most wave breaking occurs on the offshore side and on top of

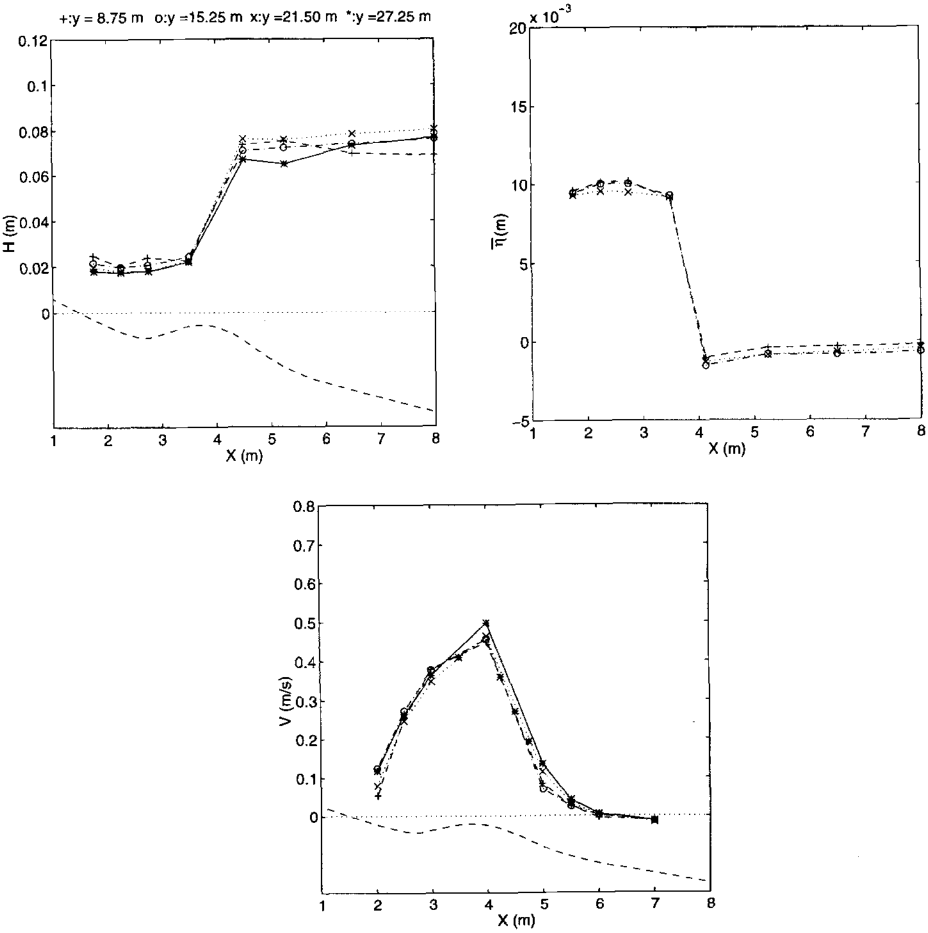


Fig. 3. Cross-shore profiles of wave height, set-up of the mean water level and longshore current velocity at four transects, test SA243. Additional measurement of longshore current velocity at fourth transect ($y = 27.25$ m) included. The bottom profile is given as a reference.

the bar, followed by a nonbreaking area in the trough and then some additional breaking near the water line. The breaking occurs in a narrow strip of about two wave lengths, in which the wave height shows a steep decline. The wave height transformation is shown at four transects at various positions with respect to the inflow denoted by $y$, demonstrating that the wave field is approximately uniform along the basin.

The set-up of the mean water level can be seen to be virtually uniform alongshore. This is important in view of the question raised in the Introduction, since it implies absence of an alongshore pressure gradient and a purely local wave-induced driving force.

The longshore current velocities show nearly uniform distributions along the beach. The pumped discharge for this specific test was 65 l/s. The width of the breaker zone is seen to be narrow compared with the width of the measured current profile. However, lateral mixing drives the current outside the area of wave forcing, causing the current profile to become smoother. The longshore current velocity has a clear maximum near the bar crest, though the measuring grid in the cross-shore direction is not dense enough to determine the exact position of the maximum. Part of the experiment was to examine the cross-shore structure of the shear instabilities. These measurements were performed with an alongshore array of twelve EMF's. The position of the alongshore array was varied with respect to the shore line. For test SA243 one EMF in the alongshore array coincided with the fourth measuring transect, resulting in additional measurements of the longshore current velocity. These are also shown in Fig. 3, indicating that the maximum longshore current velocity is indeed near the bar crest.

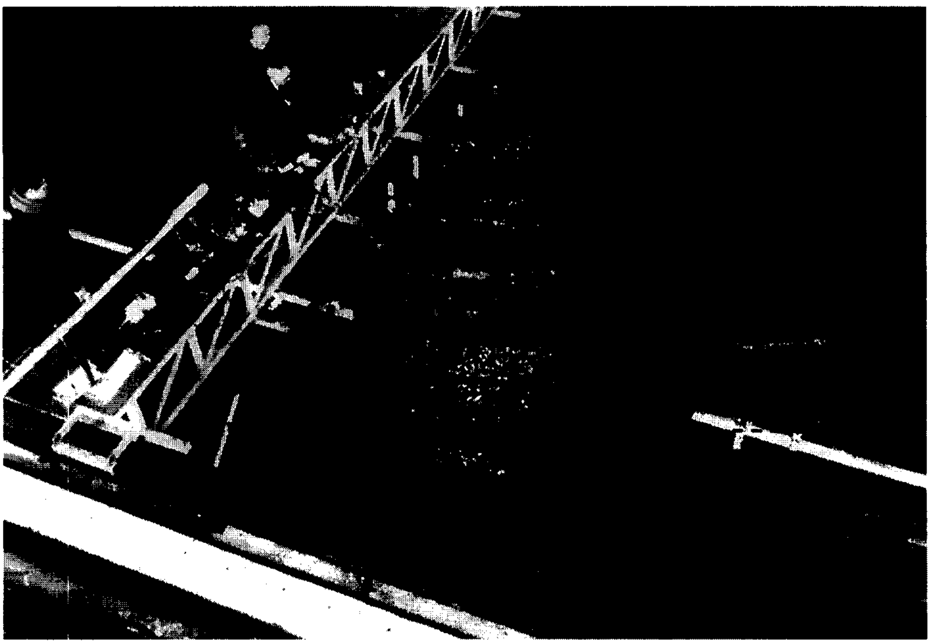

Fig. 4. Dye experiment for test SA243.

The current velocity close to the shoreline cannot be measured directly with the EMF's due to the limited water depth. The EMF's require a minimum submergence of about 1 cm and should not be closer to the bottom than 2 cm. This means that it is not possible to measure velocities at water depths smaller than 3 cm. To obtain qualitative information on the current velocity profile at small depths, i.e. near the shoreline, dye was used.

The dispersion of dye for test SA243 is shown in Fig. 4. The dye was inserted from the measurement carriage across the surfzone starting at the shore line with the picture taken shortly after. It clearly shows the high alongshore velocities on top of the bar (note the breaker line) and small velocities in the trough. In addition we can see a second maximum in the longshore current profile near the water line. These observations lend support to the theory that in case of predominantly wave driven currents the maximum

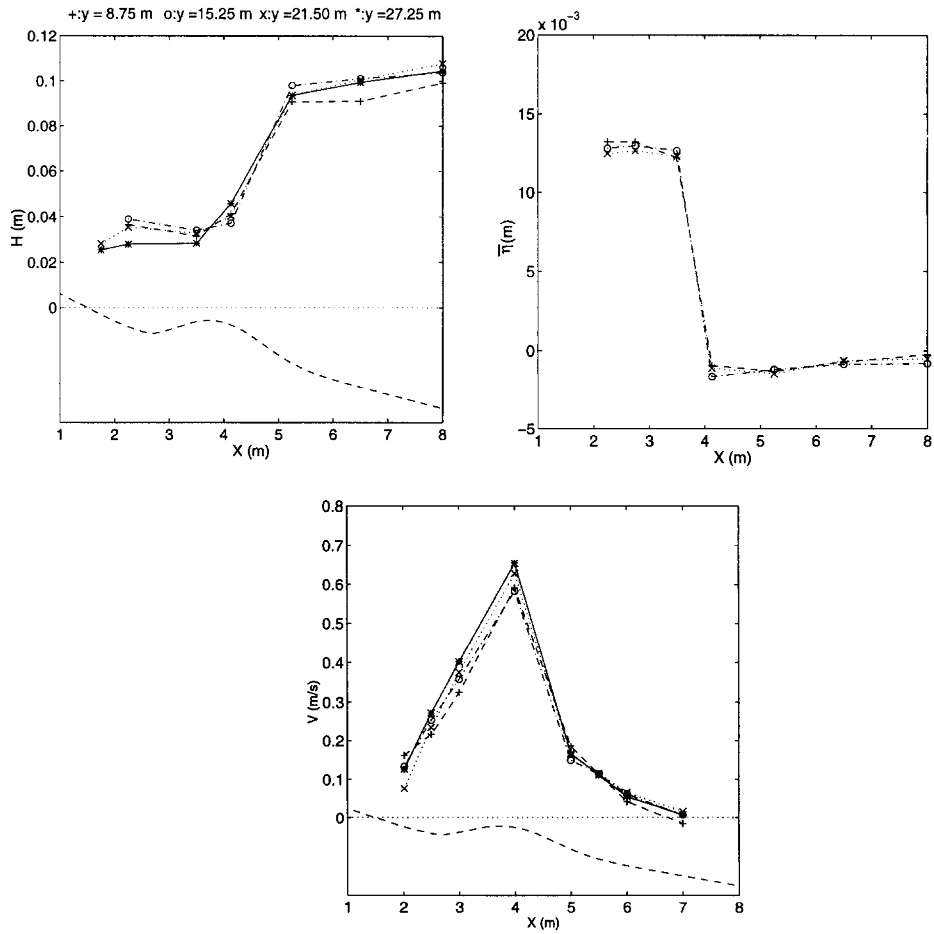


Fig. 5. Cross-shore profiles of wave height, set-up of the mean water level and longshore current velocities opening, test SA337. The bottom profile is given as a reference.

velocities are where wave breaking occurs, ie. near the bar crest and near the water line, resulting in a bimodal longshore current velocity profile.

The results for an increased wave height (10 cm), test SA337, are shown in Fig. 5. The wave period is kept at 1 second. The wave field is again shown to be approximately uniform with maximum differences in wave height offshore in the order of 10%. The set-up of the mean water level is increased, but the alongshore differences in the set-up are still negligible. Due to the increased wave height, wave breaking starts further offshore, resulting in a slightly broader current velocity profile (compare Figs. 3 and 5). The wave height in the trough is about 50% larger than in the previous case due to the increased set-up level. The 25% increase in incident wave height results in a 25% increase of the maximum measured longshore current velocity on top of the bar (Fig. 5)

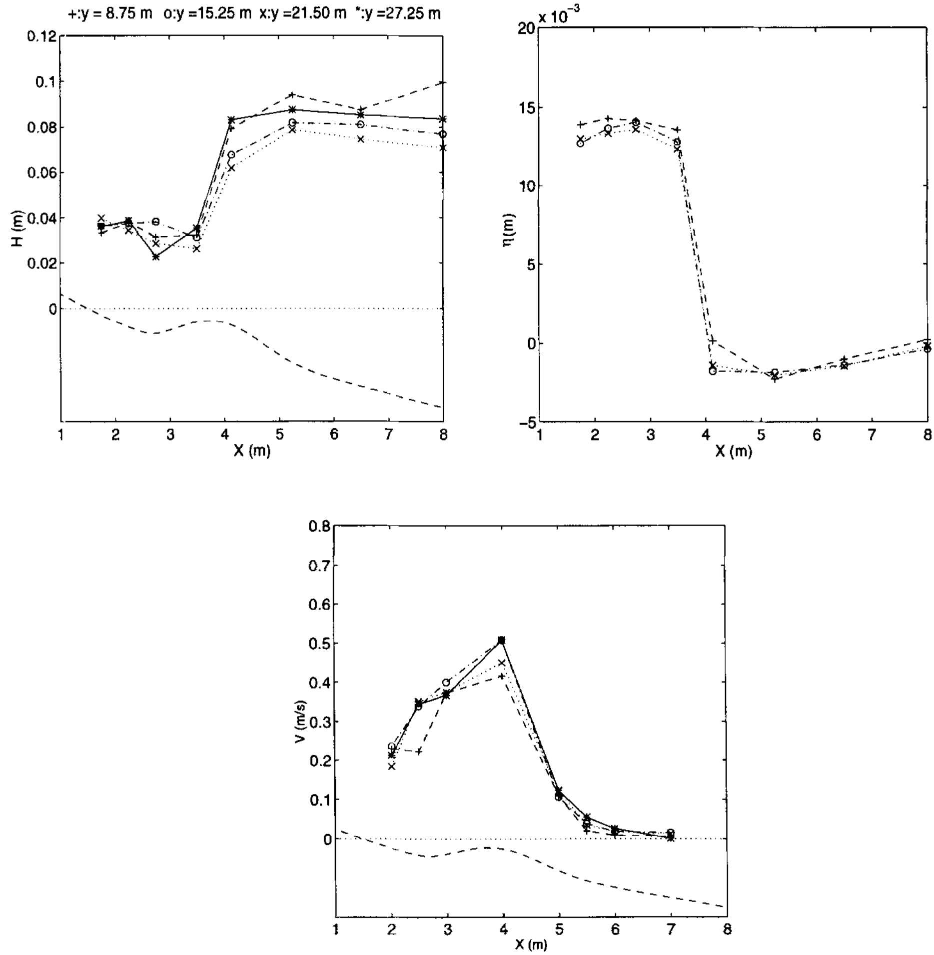


Fig. 6. Cross-shore profiles of wave height, set-up of the mean water level and longshore current velocities, test SA537. The bottom profile is given as a reference.

and in a 40% increase in the wave driven longshore current mass flux, corresponding to a pumped discharge of 90 l/s.

Fig. 6 shows results for test SA537, with a wave height of 8 cm and a period of 2 seconds. The wave field is less uniform in this case. Especially near the inflow opening there are some unexpected variations in wave height. We expect this to be due to the interaction of the incident waves with the inhomogeneous current velocity field. The inhomogeneity is apparent from the measured cross-shore distributions of the longshore current velocities, where the current in the first transect clearly has a different velocity profile than in the other transects, indicating that the cross-shore distribution of the pumped inflow discharge is not correct. The redistribution of the longshore current then causes flows in the cross-shore direction, which interact with the incident waves. Further downstream the flow and wave field become more homogeneous. The comparison with

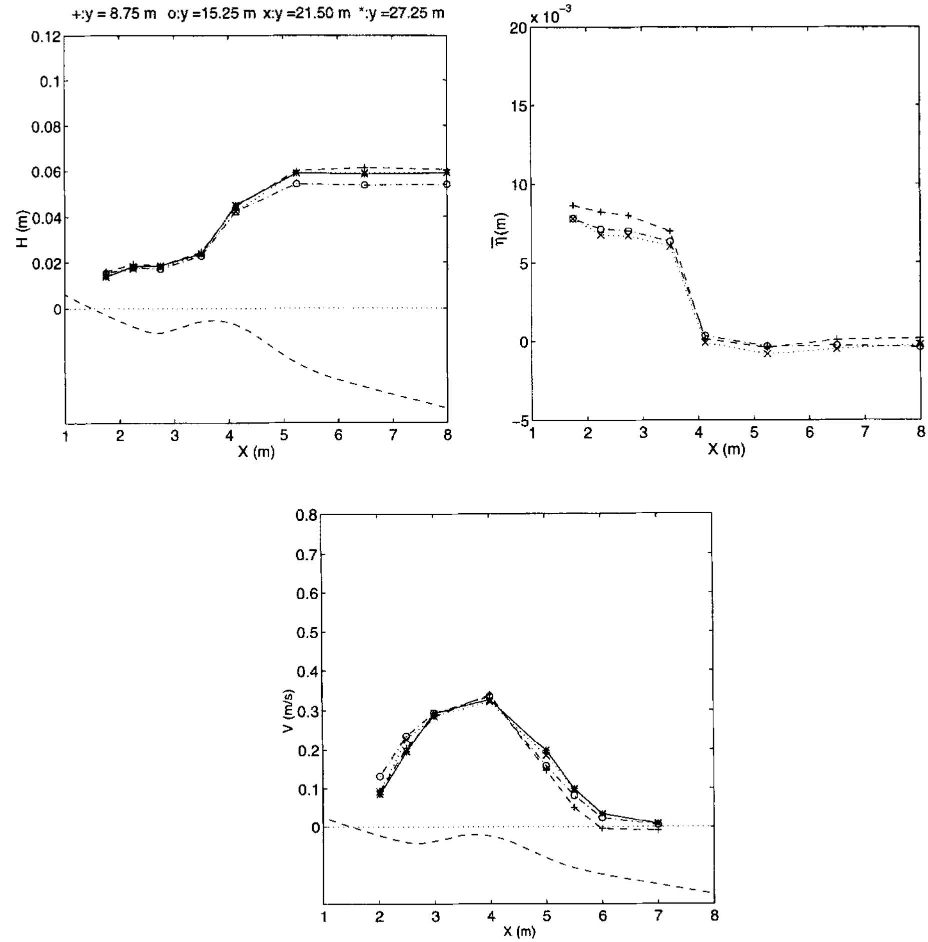


Fig. 7. Cross-shore profiles of wave height, set-up of the mean water level and longshore current velocities, test SO014. The bottom profile is given as a reference.

test SA243 shows that for test SA537 the wave height in the trough is higher, again due to the increased set-up level (compare Figs. 3 and 6). The results for the current velocity show that increasing the wave period at constant wave height causes the longshore current velocity inshore of the bar to increase, indicating that the region of wave-forcing is extended further away from the bar crest, though the wave height transformation is similar in both cases. Offshore the current velocity profiles are similar.

The results in the case of random waves, test SO014, are shown in Fig. 7. The wave field again is approximately homogeneous. The breakerzone is now in the order of 3 wavelengths. The alongshore gradient in the set-up near the inflow opening has increased but is still small ($O(10^{-4})$) m.

The longshore current velocity profile is smoother than in the monochromatic wave

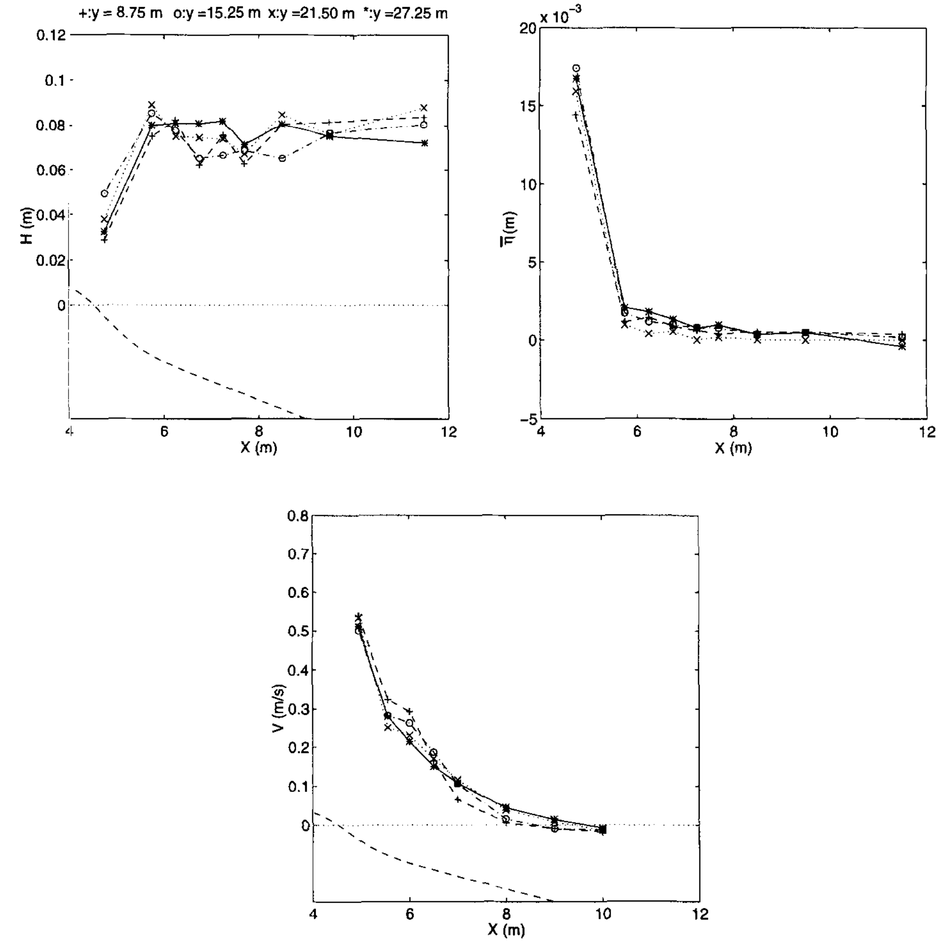


Fig. 8. Cross-shore profiles of wave height, set-up of the mean water level and longshore current velocities, test SC219. The bottom profile is given as a reference.

cases (see Fig. 7), as is to be expected due to the varying wave height and corresponding position of wave breaking, i.e. the forcing of the longshore current is spread over a broader area. The maximum longshore current velocity is less than in both previous cases, whereas offshore, the longshore current velocity is larger. Still, the maximum current velocity is on top of the bar and clearly not in the trough.

### 4.2. Non-barred profile

The results in the case of a non-barred beach, test SC219, are shown in Fig. 8. Wave breaking occurs in a narrow strip close to the shoreline, which is confirmed by the measured set-up, starting at or beyond the next to last measuring point. The wave field is less uniform compared with most of the previous cases.

It proved to be difficult to obtain a uniform longshore current in case of a non-barred beach. The longshore current profile in the first two transects shows that the distribution of the pumped discharge at the inflow opening was not optimal. Further downstream the longshore current becomes more homogeneous. The maximum current velocity occurred close to the shoreline at a depth smaller than the minimum measuring depth for the EMF. It is apparent from the measurements that there is strong lateral mixing which drives the current outside the surfzone. Comparison of the results for the barred and the plane beach, tests SA243 and SC219, suggests that the latter has an increased spatial lag between the onset of wave breaking and the longshore current velocity maximum. This is unlikely given the similarity in wave conditions and beach slope, and may be explained by the limited measurement resolution in the narrow strip near the shore line where wave breaking occurs.

## 5. Numerical modelling

### 5.1. Introduction

In the next section the equations used to model the random wave transformation, set-up and longshore current velocity will be presented. Existing state of the art model equations, based on the assumption of alongshore uniformity, have been used; no attempt has been made to improve the formulations. It is assumed that the wave transformation can be modelled with the concept of surface rollers. The idea is that the organised wave energy released at breaking, is first transferred to energy of a roller which rides on the wave front with the phase speed of the waves. The difference in velocity between the roller and the water particles at the wave front yields a shear stress between the roller and the underlying wave front. The work done by the shear stress equals the dissipation of roller energy. The time needed for the organised wave energy to dissipate through the roller causes a spatial lag between the location of wave breaking and the actual dissipation (Nairn et al., 1990).

The roller acts on the set-up of the mean water level through the cross-shore momentum balance. This results in three coupled differential equations to model the wave transformation, being the time-averaged wave energy balance, the energy balance for rollers in breaking waves and the cross-shore momentum balance to compute the set-up of the mean water level. The three equations are solved by numerical integration over the cross-shore profile, resulting in the cross-shore distribution of wave height, set-up and shear stress. The longshore current profile is then computed from the depth averaged longshore momentum balance. Comparison between computational results and measurements is used to assess the effects of rollers, bottom friction and mixing on the cross-shore distribution of the longshore current velocity.

First the equations to model the wave transformation are introduced. The measurements of wave height and set-up are used for calibration of model coefficients and verification. Next the equations to compute the longshore current velocity are introduced, again followed by comparison with the measurement data. To compare the model results with the measurements, a single test has been selected: test SO014, random waves with $H_{\rm rms} = 7$ cm, a peak period $T_{\rm p}$ of 1.2 s and a 30° angle of incidence.

### 5.2. Wave transformation

The first differential equation is the energy balance for the wave energy, $E_{\rm w}$:

$$\frac{\mathrm{d}}{\mathrm{d}x}\left(E_{\rm w} c_{\rm g} \cos(\theta)\right) = S \tag{1}$$

where $x$ is in the direction of the shore normal, positive towards the shoreline, $c_{\rm g}$ is the group velocity, $\theta$ the angle of incidence with respect to the shore normal and $S$ the dissipation term. The dissipation is modelled according to Battjes and Janssen (1978):

$$S = \frac{\rho g}{4T_{\rm p}} \alpha H_{\rm max}^2 Q_{\rm b} \tag{2}$$

where $\rho$ is the density of water, $g$ the gravitational acceleration, $T_{\rm p}$ the peak period, $\alpha$ a coefficient of O(1). The fraction of breaking waves, $Q_{\rm b}$, is computed from the implicit relation:

$$Q_{\rm b} = \exp\left(\frac{1 - Q_{\rm b}}{(H_{\rm rms}/H_{\rm max})^2}\right) \tag{3}$$

where $H_{\rm rms}$ represents the root mean square wave height and the maximum wave height, $H_{\rm max}$, is given by:

$$H_{\rm max} = \frac{0.88}{k} \tanh\left(\frac{\gamma k h}{0.88}\right) \tag{4}$$

Here $k$ is the wave number, $h$ is the total water depth including the set-up of the mean water level and $\gamma$ is a wave breaking parameter representing saturation. The wave incidence angle is obtained from Snell's law:

$$\frac{\sin(\theta)}{c} = \frac{\sin(\theta_0)}{c_0} \tag{5}$$

where $c$ represents the wave phase speed and the subscript, 0, denotes a reference point outside the surfzone. The phase speed is given by:

$$c=\frac{\omega}{k} \tag{6}$$

where $\omega$ is the angular frequency. Given the bottom profile, the wave number can be obtained from the linear wave dispersion relation:

$$\omega_2 = gk\tanh(kh) \tag{7}$$

The group velocity is given by:

$$c_{\mathrm{g}}=\frac{\mathrm{d}\omega}{\mathrm{d}k}=\left(\frac{1}{2}+\frac{kh}{\sinh(2kh)}\right)c \tag{8}$$

The dissipation of organised wave energy, $S$, serves as a source term in the second differential equation, used to compute the roller energy, $E_{\mathrm{r}}$ (Stive and De Vriend, 1994):

$$-S-\frac{d(2E_r c\cos(\theta))}{dx}=c\bar{\tau}_t \tag{9}$$

where $\bar{\tau}_t$, represents the shear stress between the roller and wave interface. The shear stress for a steady roller is given by (Duncan, 1981):

$$\bar{\tau}_t=\frac{\rho g A\sin(\beta)}{L} \tag{10}$$

$\beta$ representing the slope of the wave front and $A$ the roller area. The roller area is related to the roller energy by (Svendsen, 1984):

$$E_r=\frac{\rho A c^2}{2L} \tag{11}$$

leaving a single unknown in Eq. (9), $E_{\mathrm{r}}$, which is taken to be zero at the offshore boundary.

The storage of wave energy and momentum depends on the value of $\beta$. Large values correspond to instantaneous dissipation, resulting in a small roller areas, and vice versa. The wave slope is not known a priori, but the cross-shore momentum equation can be used to obtain a good estimate, given the fact that the roller contributes to the set-up of the mean water level.

The wave and depth averaged momentum equation in the cross-shore direction including the roller, used to compute the set-up of the mean water level, is given by (Svendsen, 1984):

$$\frac{\mathrm{d}S_{xx,\mathrm{w}}}{\mathrm{d}x}+\frac{\mathrm{d}S_{xx,\mathrm{r}}}{\mathrm{d}x}+\rho g h\frac{\mathrm{d}\bar{\eta}}{\mathrm{d}x}=0 \tag{12}$$

where $\bar{\eta}$ represents the set-up of the mean water level. The first term represents the gradient in radiation stress associated with the wave motion, the second is the roller contribution and the third term is due to the pressure gradient associated with the set-up. The wave component of the radiation stress is given by:

$$S_{xx,w} = \left(\frac{c_g}{c}(1+\cos^2\theta) - \frac{1}{2}\right)E_w \tag{13}$$

The wave averaged roller momentum flux is given by (Svendsen, 1984):

$$S_{xx,r} = 2E_r\cos^2(\theta) \tag{14}$$

The model requires boundary conditions for the wave energy, $E_w$, the roller energy, $E_r$, the set-up, $\overline{\eta}$ and a bottom profile. In addition a number of coefficients have to be defined, viz. two wave breaking parameters, $\alpha$, which is set at 1, and $\gamma$ which is obtained from (Battjes and Stive, 1985):

$$\gamma = 0.5 + 0.4\tanh\left(33\frac{H_{rms,0}}{L_0}\right) \tag{15}$$

### 5.2.1. Comparison with data

The result for the wave height transformation is shown in Fig. 9. The computed set-up is shown in Fig. 10. Overall, both wave height transformation and set-up compare

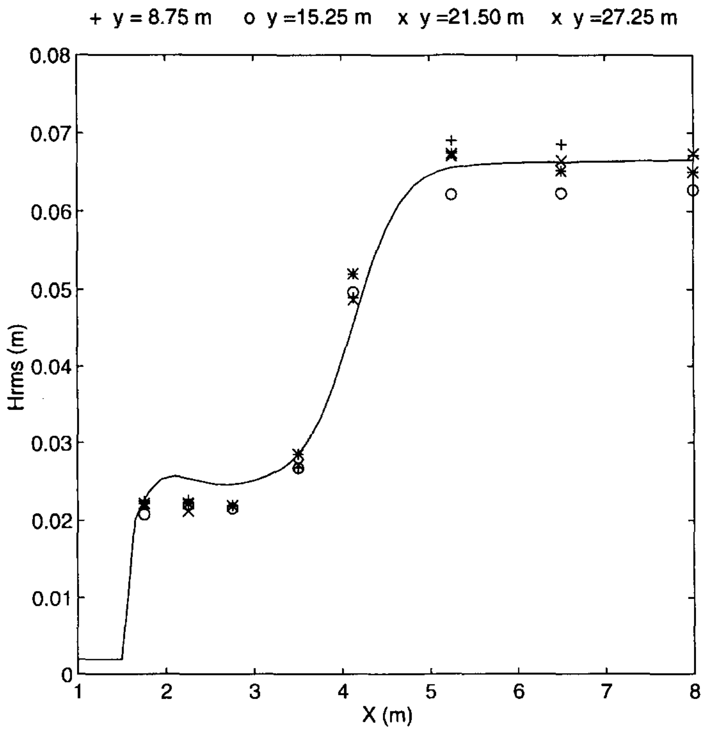


Fig. 9. Wave height transformation, comparison between computational results (solid line) and measurements.

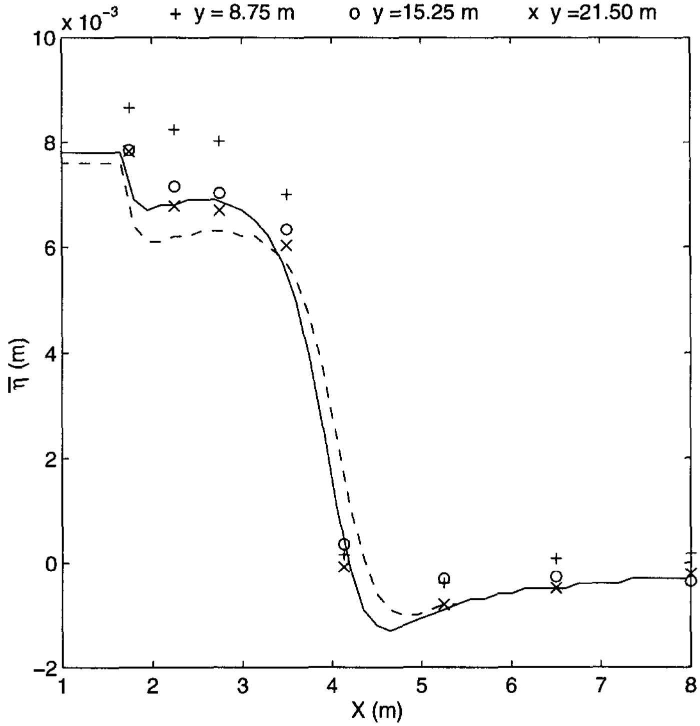


Fig. 10. Set-up of mean water level computed with (solid line) and without (dashed line) the roller contribution, compared with measurements.

favourably with the measurements. A more detailed examination shows that the wave shoaling seaward of the bar is somewhat underestimated by the model (ie. wave dissipation is overestimated). In the trough the wave height is slightly overpredicted. Still, the wave energy decay over the bar is well predicted and so is the set-up if the roller effect is included with $\beta = 0.1$. In the case where the roller is not included, the set-up level near the shore line is underestimated (Fig. 10). However, inclusion of the roller appears to cause hardly any spatial lag in the present case.

### 5.3. Longshore current

Given the cross-shore distribution of the forcing due to the breaking waves, the longshore current velocity distribution can be computed from wave-averaged and depth-integrated longshore momentum equation:

$$\frac{\mathrm{d}S_{xy}}{\mathrm{d}x} + \frac{\mathrm{d}S_{xy,\mathrm{t}}}{\mathrm{d}x} = \bar{\tau}_{y,\mathrm{b}} \tag{16}$$

where the first term represents the forcing due to wave dissipation, the second term is the horizontal mixing due to turbulence, and $\bar{\tau}_{y,\mathrm{b}}$ represents the wave-averaged bottom shear stress in the alongshore direction. Traditionally the wave forcing is obtained from linear wave theory:

$$\frac{\mathrm{d}S_{xy}}{\mathrm{d}x} = \frac{\sin(\alpha_0)}{c_0}\frac{\mathrm{d}}{\mathrm{d}x}\left(E_{\mathrm{w}}c_{\mathrm{g}}\cos(\theta)\right) \tag{17}$$

The wave forcing, including the roller contribution, is given by (Deigaard, 1993):

$$\frac{\mathrm{d}S_{xy}}{\mathrm{d}x} = \frac{\sin(\theta)}{c}\rho\frac{\mathrm{d}}{\mathrm{d}x}\left(E_{\mathrm{w}}c_{\mathrm{g}}\cos(\theta) + 2E_{\mathrm{r}}c\cos(\theta)\right) = \bar{\tau}_{\mathrm{t}}\sin(\theta) \tag{18}$$

The turbulence contribution in Eq. (16) is modelled as a diffusion term (Longuet-Higgins, 1970):

$$\frac{\mathrm{d}S_{xy,t}}{\mathrm{d}x} = \rho\frac{\mathrm{d}}{\mathrm{d}x}\left(h\nu_{\mathrm{t}}\frac{\mathrm{d}V}{\mathrm{d}x}\right) \tag{19}$$

introducing $V$ as the depth-averaged longshore velocity and $\nu_{\mathrm{t}}$ as the horizontal eddy viscosity, which is modelled according to (Battjes, 1975):

$$\nu_{\mathrm{t}} = H_{\mathrm{rms}}\left(\frac{P}{\rho}\right)^{1/3} \tag{20}$$

where the turbulent kinetic energy is generated by the shear stress at the trough level:

$$P = c\bar{\tau}_{\mathrm{t}} \tag{21}$$

The (non-linear) bottom shear stress is modelled as:

$$\bar{\tau}_{\mathrm{y,b}} = \frac{1}{T_{\mathrm{p}}}\int_0^{T_{\mathrm{p}}}\rho c_{\mathrm{f}}\sqrt{\left(\tilde{u}^2 + 2\tilde{u}V\sin(\theta) + V^2\right)}\,(V + \tilde{u}\sin(\theta))\,\mathrm{d}t \tag{22}$$

where $c_{\mathrm{f}}$ is a friction coefficient and $\tilde{u}$ the instantaneous wave orbital velocity, obtained from the local $H_{\mathrm{rms}}$, in the direction of wave propagation. In the computations, $c_{\mathrm{f}}$ is used as a fit parameter. The whole set results in an implicit second order differential equation in $V$, which is solved iteratively; boundary conditions are provided by setting $V$ to zero offshore and at the shoreline.

#### *5.3.1. Comparison with data*

The measurements for the longshore current velocity were performed at one third of the water depth from the bed, which in the case of a logarithmic velocity profile is representative for the depth-averaged flow. However, it is not known whether the velocity profiles are actually logarithmic, so the measured velocities may differ from the depth averaged velocity. In the comparison between measurements and model results, it is assumed that these differences are small.

The results for the computed longshore velocities, using $c_{\mathrm{f}} = 0.007$, show good agreement with the measurements (see Fig. 11). The cross-shore distribution of the longshore current velocity profile matches the measured distribution quite well. In particular, the location and the value of the computed and measured maximum longshore current velocity coincide. This shows the ability to predict the longshore current velocity

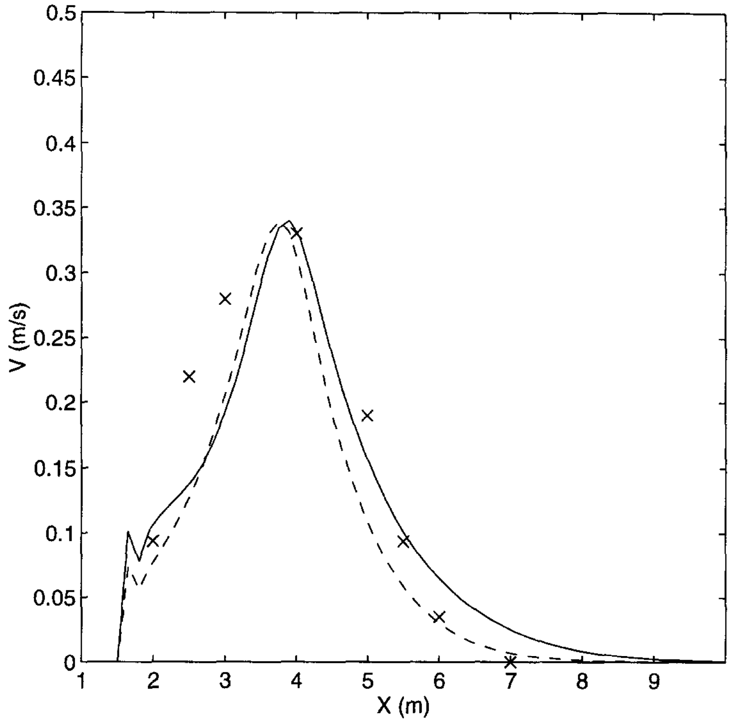


Fig. 11. Computed longshore current velocities for linear, $c_f = 0.015$ (dashed line) and non-linear, $c_f = 0.007$ (solid line) bottom shear stress, compared with measurements at $y = 21.50$ m from the inflow opening ($x$).

profiles for purely wave driven flows on barred beaches, using existing model equations for longshore uniform conditions.

A closer look at the results shows that the longshore current velocities are overpredicted at the seaward end of the bar and underpredicted in the trough. It is difficult to say what causes these differences, given the fact that forcing, mixing and bottom friction have similar order effects on the predicted current velocities in these areas. These effects are examined in more detail below.

The sensitivity of the computed longshore current velocity to the bottom shear stress formulation is illustrated by the use of a simpler, linear bottom friction. Often the bottom shear stress is linearised under the assumptions that the longshore current velocity is small compared to the wave orbital velocity and that the angle of incidence is small (Longuet-Higgins, 1970):

$$\bar{\tau}_{y,b} = \rho c_f \overline{|\tilde{u}|} \sin(\theta) V \tag{23}$$

These assumptions are violated in the case presented, but the idea is to investigate the importance of the bottom shear stress formulation. The bottom friction coefficient, $c_f$, has been increased to 0.015 to give the same maximum current velocity as in the non-linear case. The results, see Fig. 11, show fairly good agreement with the measurements both for the linear and non-linear bottom shear stress formulations. Only minor differences in the longshore current velocity occur, similar to the results obtained by Thornton and Guza (1986).

The roller effect on the longshore current velocity profile is illustrated in Fig. 12. If the roller contribution is excluded from the longshore momentum balance, i.e. using Eq. (17) to compute the forcing of the longshore current, the measured and computed maxima no longer coincide. This shows that the cross-shore distribution of the shear stress can only be modelled correctly if the roller contribution is taken into account. Note that mixing has no significant impact on the position of maximum velocity (see Fig. 12). The absence of storage of alongshore directed momentum in the model without roller results in a premature release of this momentum, resulting in an underestimation of the longshore current velocities in the trough. If mixing is included, only part of this effect is compensated, but it also leads to an overestimation of the current velocities offshore.

From the current velocity distributions shown in Fig. 12 it becomes also obvious that mixing has a significant effect. It is often assumed that in case of random waves, no additional mixing is required to model the longshore current velocity profile. In this case

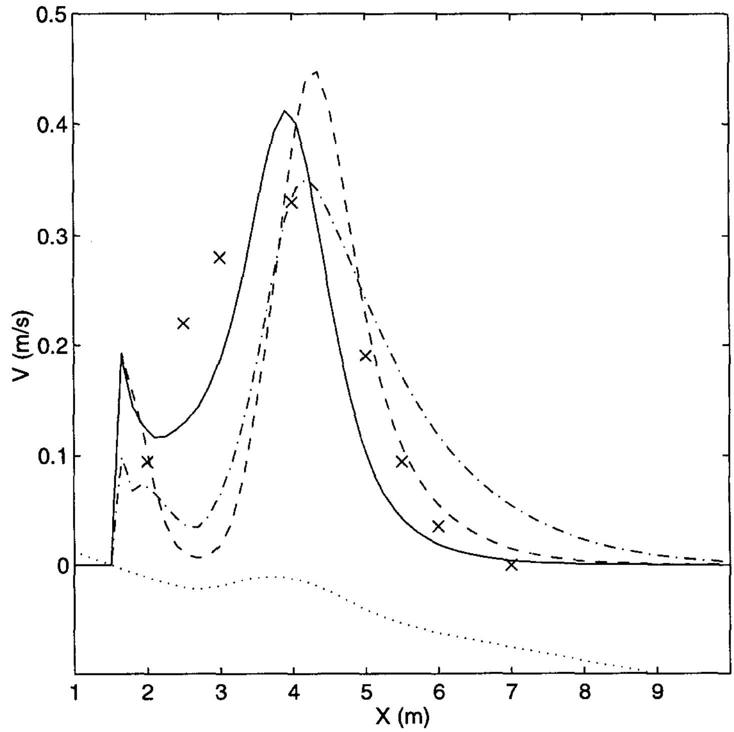


Fig. 12. Intercomparison of computed longshore current velocities without mixing (solid line), without a roller (dash-dotted line), without a roller and without mixing (dashed line). Non-linear bottom shear stress with a friction coefficient, $c_f$, of 0.007. Measured longshore current velocities at $y = 21.50$ m from the inflow opening ($x$).

however, the predicted longshore currents are clearly too narrow compared to the measurements if mixing is not included. It seems therefore that in the case of random waves on a barred beach the lateral mixing effect is more important than in the case of random waves on a plane beach. This is ascribed to the fact that in the case of a plane beach there is a gradual increase and decrease in the wave forcing as the water depth decreases, whereas on a barred beach there is concentrated wave breaking on the bar followed by a rapid decrease in the number of breaking waves in the trough, resulting in stronger shears and thereby increased mixing.

Overall, it appears that both roller and lateral mixing have effects on the longshore current profile of comparable magnitude but of a different kind: the roller shifts the profile shoreward and mixing smears it out. Both are needed to obtain reasonable agreement with the measured profile.

## 6. Discussion

The cross-shore distribution of the longshore current velocities for purely wave-driven currents has been examined. It has been shown that in absence of an alongshore pressure gradient the maximum longshore current velocities occur where breaking is most intense, i.e. on the bar and near the shoreline. Lateral mixing smooths the current profile, but does not significantly affect the position of the maximum current velocity, which in the case of a barred beach clearly remains near the crest. This holds for the cases of short waves (test SA243), long waves (test SA537) and random waves (test SO014) on barred beaches. This leads us to believe that the occurrence of the maximum longshore current velocities in the trough, as observed during the DELILAH field experiment at Duck, North Carolina, are not the result of pure local wave forcing.

The comparison between measurements and computational results has demonstrated the ability to model purely wave driven longshore currents on barred beaches, using existing model equations. Note that longshore currents in the field are in general not locally wave driven only, but result from a variety of different mechanisms, including wind and pressure gradients.

## 7. Conclusions

A comprehensive set of data, consisting of current velocity measurements on both barred and non-barred beaches, as well as wave transformation and set-up data, has been established. The data can be used for verification and validation of numerical models.

The results for the measured set-up show that the alongshore pressure gradients in most of the cases were negligible compared to the wave forcing, indicating that the measured current velocity profiles correspond to purely wave-driven currents.

In the case of forcing by monochromatic waves on a barred beach, the maximum of the longshore current velocity was clearly near the bar crest, coinciding with the location where waves are breaking. The dye experiment shows that in this case a second maximum in the longshore current velocity occurred near the shoreline, where the remaining wave energy was dissipated after propagating over the bar.

In the case of random waves on a barred beach, the longshore current velocity profile became smoother, but the maximum longshore current velocity was still near the bar crest and clearly not in the trough.

The longshore current velocity in the trough increased if the wave period or the wave height were increased, indicating that the wave forcing was extended toward the shore.

For monochromatic waves on a plane beach the maximum alongshore current velocity occurred very close to the water line, at a depth smaller than the minimum depth for instrument deployment. Strong mixing caused the velocity profile to smooth out, becoming of comparable width as the current velocity profiles in the case of a barred beach.

Comparison of computational results with measurements showed good agreement for wave transformation, set-up and longshore current velocity profiles. This demonstrates the ability to model purely wave driven longshore currents with existing model equations.

Lateral mixing was required to obtain a good match with the data. This showed that the randomness of the incident wave field by itself could not account for the necessary smoothing of the longshore current profile in the case of a barred beach.

The transition effect, caused by the surface roller, was important in the correct prediction of the location of maximum wave forcing. In addition, the delayed release of alongshore wave momentum caused a significant increase in the longshore current velocity in the trough. However, inclusion of the roller effect does not shift the longshore current velocity maximum on a barred beach to the deepest part of the trough.

Summarising, the preceding conclusions imply that in absence of an alongshore pressure gradient the maximum longshore current velocity occurs near the areas of most intense breaking, and that the occurrence of velocity maxima in the trough, as frequently observed in field experiments, can be ascribed to the presence of an alongshore pressure gradient (excluding wind effects).

## Acknowledgements

The experiments, performed in the large multidirectional wavebasin at Delft Hydraulics, were funded by the European Community in the framework of the Large Installations Plan (LIP), project 19M. A.R. is funded by the J.M. Burgers Centre for Fluid Mechanics, The Netherlands. He thanks Paul Visser (Delft University of Technology) for his valuable comments on the experimental set-up.

## References

Battjes, J.A., 1975. Modelling of turbulence in the surfzone. In: Proc. Symp. Model. Techniques, San Francisco, CA, pp. 1050–1061.

Battjes, J.A. and Janssen, J.P.F.M., 1978. Energy loss and set-up due to breaking in random waves. In: Proc. 16th Coastal Eng. Conf., Hamburg, pp. 569–587.

Battjes, J.A. and Stive, M.J.F., 1985. Calibration and verification of a dissipation model for random breaking waves. J. Geophys. Res., 90: 9159–9167.